Electronic Supplementary Information for

# 3D superhydrophobic reduced graphene oxide for activated $NO_2$ sensing with enhanced immunity to humidity

Jin Wu, ‡*[a] Zhong Li, ‡[b] Xi Xie, [a] Kai Tao, [c] Chuan Liu, *[a] Khiam Aik Khor, [b] Jianmin Miao *[b] and Leslie K. Norford [de]

[a]State Key Laboratory of Optoelectronic Materials and Technologies and the Guangdong Province Key Laboratory of Display Material and Technology, School of Electronics and Information Technology, Sun Yat-sen University, Guangzhou 510275, China.

[b]School of Mechanical and Aerospace Engineering, Nanyang Technological University, Singapore 639798, Singapore

[c]The Ministry of Education Key Laboratory of Micro and Nano Systems for Aerospace, Northwestern Polytechnical University, Xi'an, 710072, China.

[d]Center for Environmental Sensing and Modeling (CENSAM), Singapore-MIT Alliance for Research and Technology (SMART) Centre, Singapore 117543, Singapore

[e]Department of Architecture, Massachusetts Institute of Technology, Cambridge, MA 02139, USA

‡ These authors contributed equally to this work

*To whom correspondence should be addressed. E-mail: wujin8@mail.sysu.edu.cn; liuchuan5@mail.sysu.edu.cn or MJMMiao@ntu.edu.sg, Tel., (+65) 6790 6038

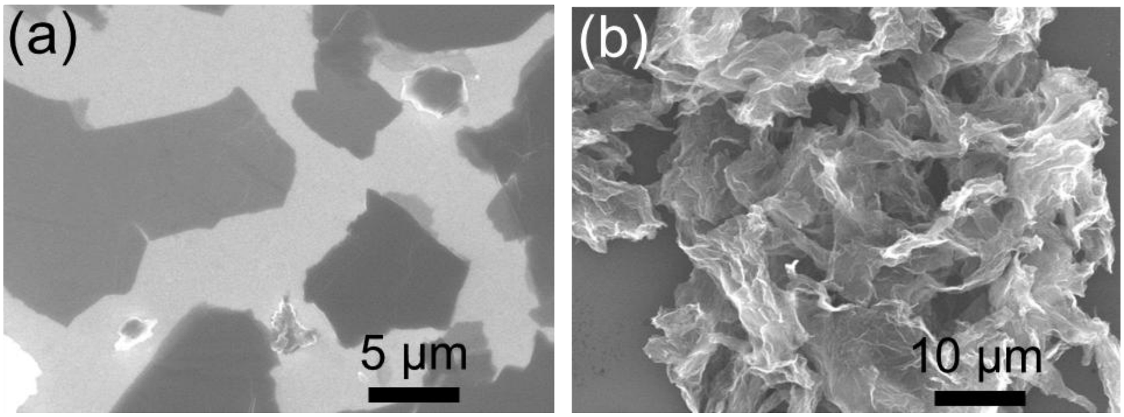


Figure S1 SEM images of 2D GO sheets (a) and 3D RGO hierarchical structures (b) respectively.

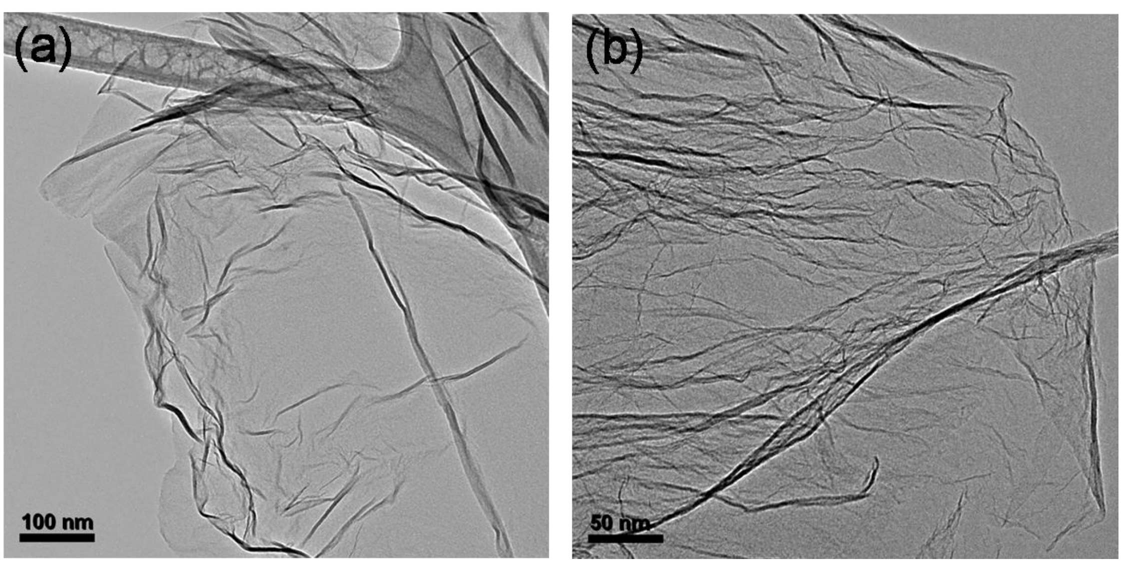


Figure S2 TEM images of SPS-synthesized RGO sheets, which exhibited the wrinkled and corrugated morphology.

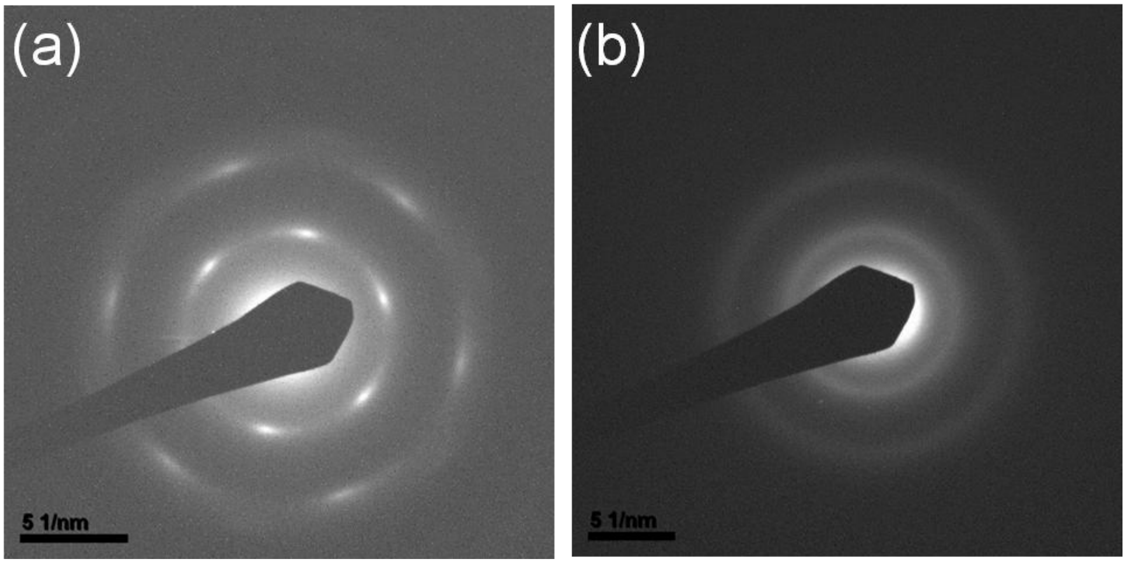


Figure S3 TEM selected area electron diffraction (SAED) patterns of GO (a) and RGO (b) respectively.

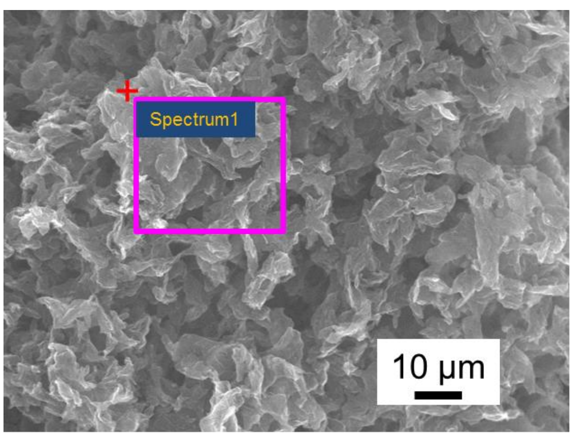


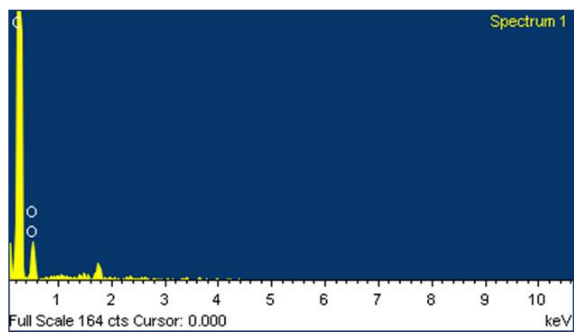


| Element | Weight% | Atomic% |
|---|---|---|
| C K | 88.71 | 91.28 |
| O K | 11.29 | 8.72 |
| Totals | 100.00 | 100.00 |

Figure S4 Energy-dispersive X-ray (EDX) spectra of RGO.

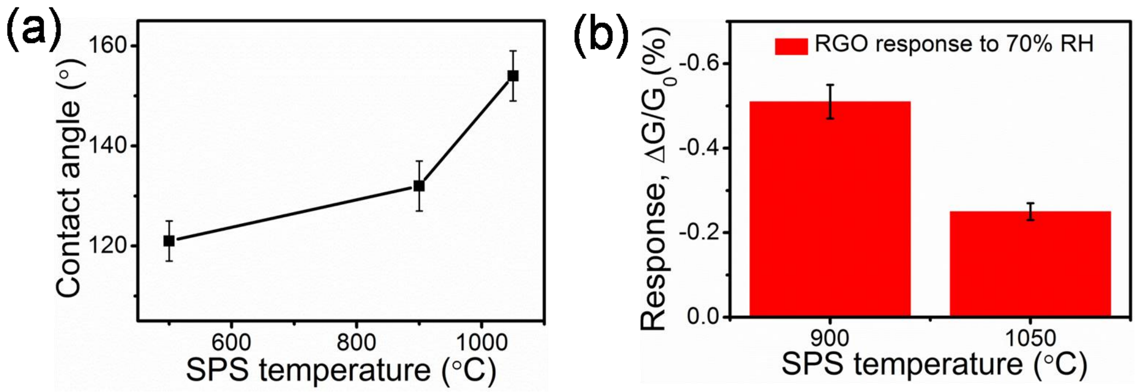


Figure S5 a) Responses to 70% RH of the RGO synthesized at two different temperatures: 900 and 1050 ℃. b) Plot of the contact angle of water droplet on RGO versus SPS temperature.

Table S1 Comparison of the contact angles of water droplet on RGO that reduced from GO by different methods

| GO reduction method | SPS This work | Hydrazine reduction[1] | Caffeic acid[2] | Hydrothermal reduction with oleylamine[3] | Aluminum reduction[4] | Thermal reduction[5] |
|---|---|---|---|---|---|---|
| Contact angle | 154 ° | 127 ° | 54.8 °- 93.3 ° | 130 ° | 90.5 ° | 72.8 ° |

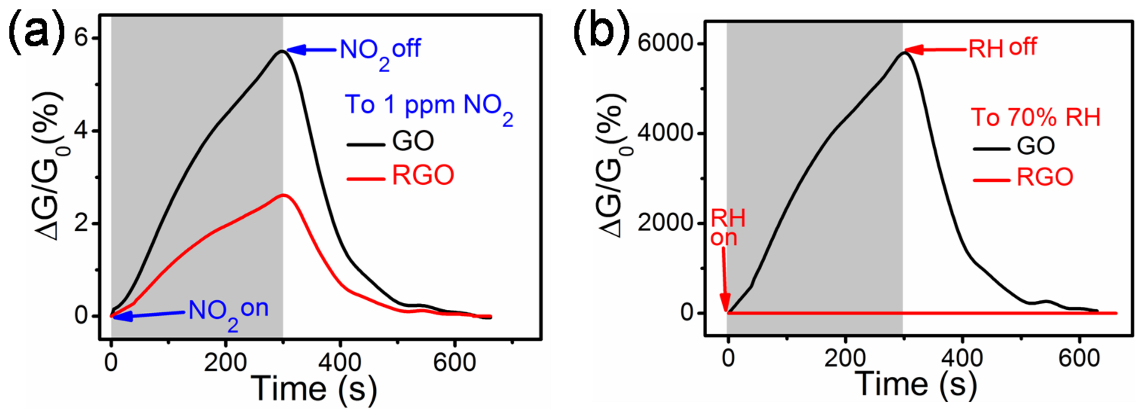


Figure S6 Dynamic responses of the GO sensor (black) and SPS synthesized RGO sensor (red) to 1 ppm $NO_2$ (a) and 70% RH (b), respectively.

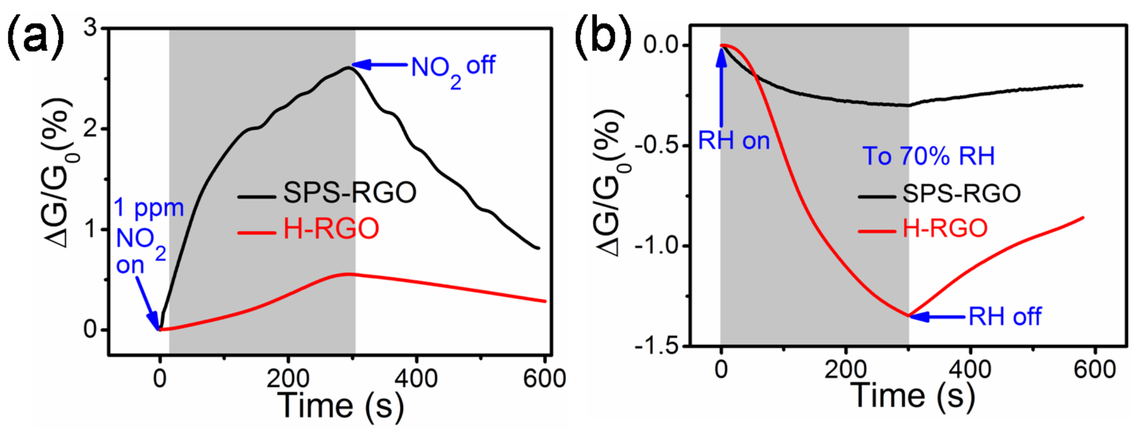


Figure S7 Dynamic responses of the SPS obtained RGO (SPS-RGO) (black) and hydrothermal synthesized RGO (H-RGO) (red) to 1 ppm $NO_2$ (a) and 70% RH (b), respectively. The H-RGO was synthesized according to our previously reported work.[6] Briefly, 100 mg hydroquinone was mixed with 10 mL 2 mg $mL^{-1}$ GO aqueous dispersion. The mixture was put into a 16 mL sealed Teflon-lined autoclave, followed by heating the system at 100 C for 10 hours.

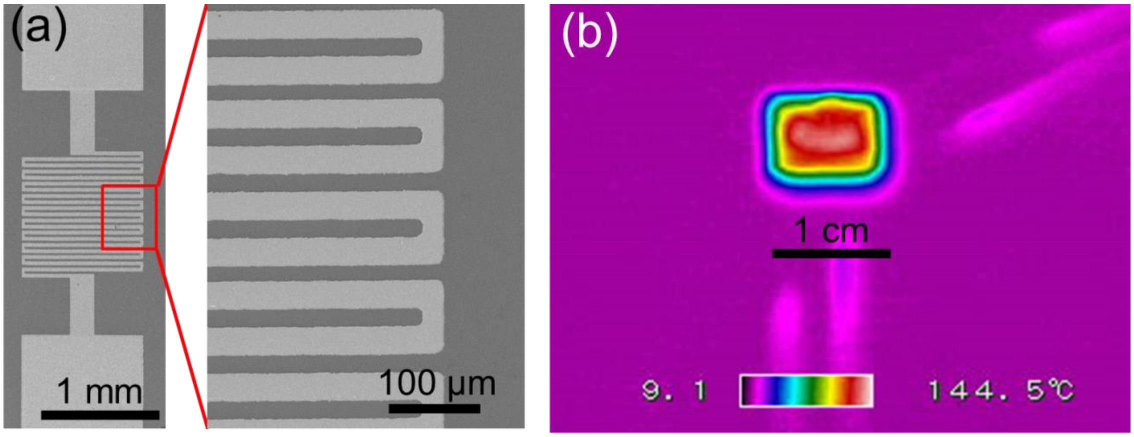


Figure S8 Characterization of the microheater. a) SEM image of a microheater (left). Two Au electrodes were fabricated on the two ends of serpentine Pt heating line. The magnified SEM image of the serpentine Pt heating line with the line width of 30 μm was shown in right side. b) An optical image captured by an infrared camera showing temperature distribution on the sensor chip when a DC voltage of 13 V was applied on the microheater. An average temperature of 140 ℃ was obtained.

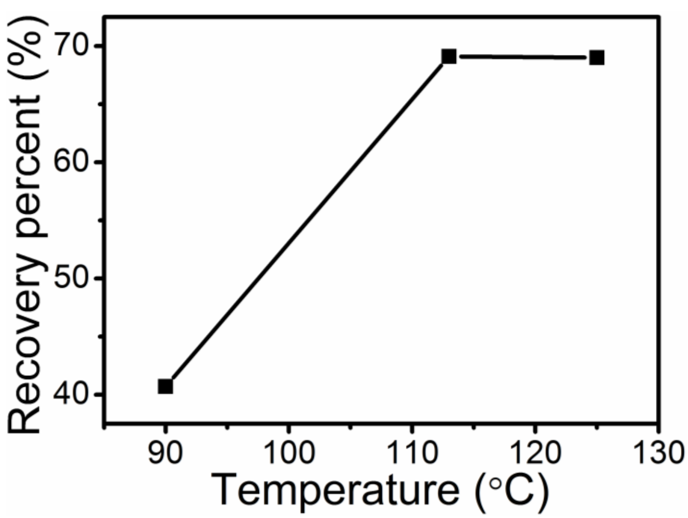


Figure S9 Plot of the recovery percent of this RGO based $NO_2$ sensor versus temperature.

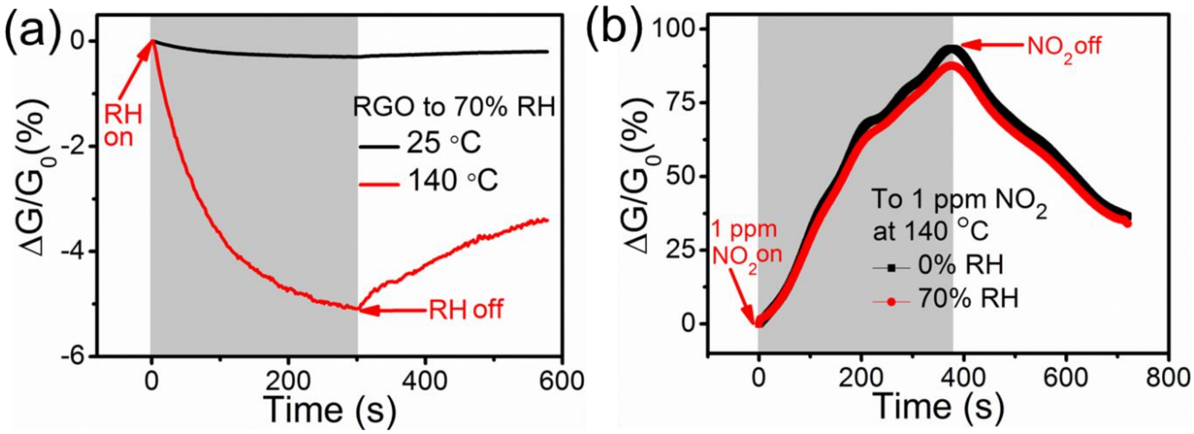


Figure S10 a) Dynamic responses of the superhydrophobic RGO to 70% RH at 25 ℃ (black) and 140 ℃ (red) respectively. b) Dynamic response variation of the superhydrophobic RGO sensor to 1 ppm $NO_2$ at 140 ℃ when the relative humidity increased from 0% (black) to 70% (red).

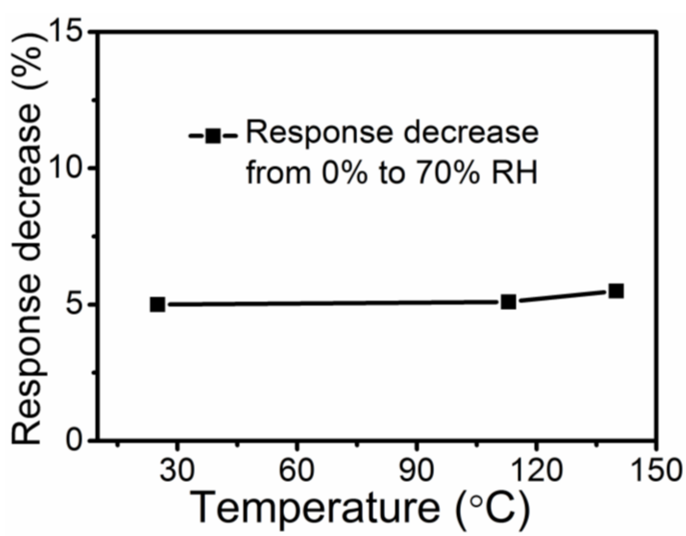


Figure S11 Plot of the response decrease of the RGO sensor from 0% to 70% RH versus substrate temperature in 1 ppm $NO_2$ detection.

**Calculation of noise level ($RMS_{Noise}$) and limit of detection (LOD) of the RGO sensor**[7, 8]

1) Perform linear fit for the response versus $NO_2$ concentration curve. The sensitivity (slope) can be obtained from the linear fit (Figure S12a).
2) Take 11 data points at the baseline of response versus time curve before exposure to $NO_2$ (*Yi*).
3) Plot the response versus time curve and then implement 5$^{th}$ order polynomial fit (Figure S12b).
4) Take the regular residual ($Y_i$-$\bar{Y}$) from polynomial fit and calculate the root-mean squared deviation ($RMS_{Noise}$) and LOD with below Equation S1 and S2:

$RMS_{Noise}\,(ppm^{-1}) = \sqrt{(V_x^2/(N-1))}$, in which $V_x^2 = \sum(Y_i-Y)^2$ (Equation S1)

$LOD\,(ppm^{-1}) = 3 \times RMS_{Noise}/Slope$ (Equation S2)

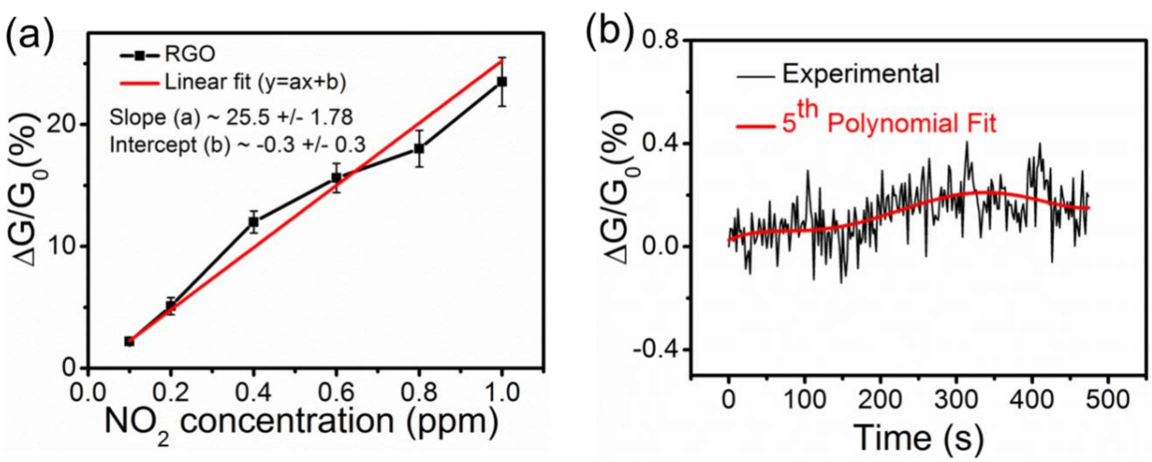


Figure S12 a) Plot of experimentally obtained (black dashed) and linearly fitted (red) response versus $NO_2$ concentration. b) The 5$^{th}$ order polynomial-fitted response of the RGO sensor versus time at the baseline before $NO_2$ exposure.

Table S2 5th order polynomial fitting data for the SPS-RGO based $NO_2$ sensor

| **Time (sec)** | $Y_i$-Y | ($Y_i$-Y)^2 |
|---|---|---|
| **40** | 0.053 | 2.81E-03 |
| **80** | -0.07706 | 5.94E-03 |
| **120** | 0.16078 | 2.59E-02 |
| **160** | -0.05588 | 3.12E-03 |
| **200** | -0.03304 | 1.09E-03 |
| **240** | 0.02978 | 8.87E-04 |
| **280** | 0.04239 | 1.80E-03 |
| **320** | 0.11791 | 1.39E-02 |
| **360** | 0.01843 | 3.40E-04 |
| **400** | 0.04664 | 2.18E-03 |
| **440** | 0.03839 | 1.47E-03 |

Table S3 Calculation of sensitivity, $RMS_{noise}$ and LOD

| **Material for $NO_2$ Sensing** | **Slope (Sensitivity) ($ppm^{-1}$)** | **Standard Error ($ppm^{-1}$)** | $V_x^2$ | $RMS_{noise}$ | **LOD (ppm)** |
|---|---|---|---|---|---|
| **Superhydrophobic 3D RGO** | 25.5 | 1.78 | 0.0594 | 0.0771 | 0.00907 |

Table S4 Comparison of different carbon nanomaterial-based $NO_2$ sensors in LOD

| **Sensing materials** | **3D-RGO-$SnO_2$[9]** | **RGO on 3D pillars[7]** | **RGO/$Cu_2O$[10]** | **CMG[11]** | **GO[12]** | **SWCNT[13]** | **Superhydrophobic 3D RGO (This work)** |
|---|---|---|---|---|---|---|---|
| **LOD (ppb)** | 2000 | 1200 | 64 | 3600 | 20 | 44 | 9.1 |

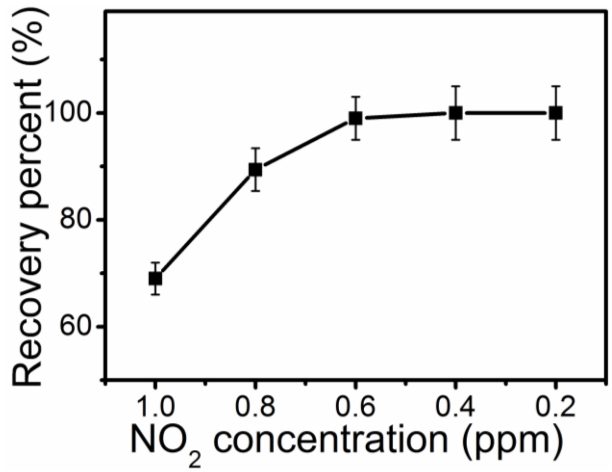


Figure S13 Plot of recovery percent variations of the RGO sensor versus $NO_2$ concentration in the reversible detection of $NO_2$ with reduced concentration from 1000 to 200 ppb.

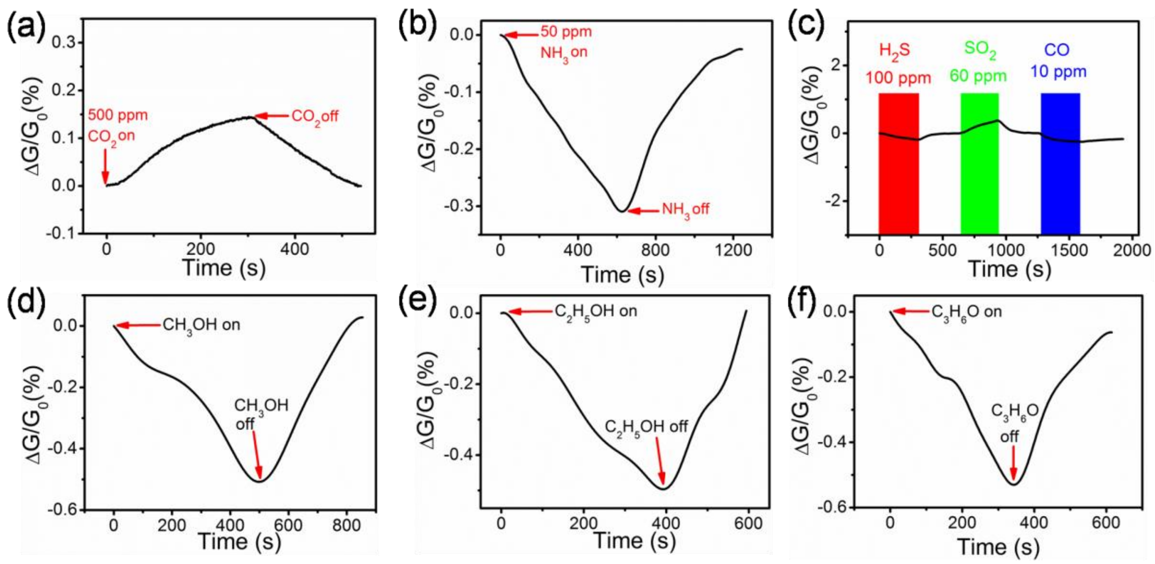


Figure S14 Dynamic responses of the superhydrophobic RGO to 500 ppm $CO_2$ (a), 50 ppm $NH_3$ (b), 100 ppm $H_2S$ (c), 60 ppm $SO_2$ (c), 10 ppm CO (c) and various saturated volatile organic compounds (VOCs), including methanol (d), ethanol (e) and acetone (f), respectively.

## References


1 S. Wang, Y. Zhang, N. Abidi and L. Cabrales, *Langmuir*, 2009, **25**, 11078-11081.

2 Z. Bo, X. Shuai, S. Mao, H. Yang, J. Qian, J. Chen, J. Yan and K. Cen, *Sci. Rep.*, 2014, **4**, 4684.

3 Z. H. Tang, Z. W. Zhang, Z. Han, S. L. Shen, J. Li and J. H. Yang, *J. Mater. Sci.: Mater. Electron.*, 2016, **51**, 8791-8798.

4 D. Y. Wan, C. Y. Yang, T. Q. Lin, Y. F. Tang, M. Zhou, Y. J. Zhong, F. Q. Huang and J. H. Lin, *ACS Nano*, 2012, **6**, 9068-9078.

5 F. Perrozzi, S. Croce, E. Treossi, V. Palermo, S. Santucci, G. Fioravanti and L. Ottaviano, *Carbon*, 2014, **77**, 473-480.

6 J. Wu, K. Tao, J. Zhang, Y. Guo, J. Miao and L. K. Norford, *J. Mater. Chem. A*, 2016, **4**, 8130-8140.

7 L. T. Duy, D.-J. Kim, T. Q. Trung, V. Q. Dang, B.-Y. Kim, H. K. Moon and N.-E. Lee, *Adv. Funct. Mater.*, 2015, **25**, 883-890.

8 V. Dua, S. P. Surwade, S. Ammu, S. R. Agnihotra, S. Jain, K. E. Roberts, S. Park, R. S. Ruoff and S. K. Manohar, *Angew. Chem. Int. Ed.*, 2010, **49**, 2154-2157.

9 L. Li, S. He, M. Liu, C. Zhang and W. Chen, *Anal. Chem.*, 2015, **87**, 1638-1645.

10 S. Deng, V. Tjoa, H. M. Fan, H. R. Tan, D. C. Sayle, M. Olivo, S. Mhaisalkar, J. Wei and C. H. Sow, *J. Am. Chem. Soc.*, 2012, **134**, 4905-4917.

11 W. Yuan, A. Liu, L. Huang, C. Li and G. Shi, *Adv. Mater.*, 2013, **25**, 766-771.

12 M. Donarelli, S. Prezioso, F. Perrozzi, L. Giancaterini, C. Cantalini, E. Treossi, V. Palermo, S. Santucci and L. Ottaviano, *2D Mater.*, 2015, **2**, 035018.

13 J. Li, Y. J. Lu, Q. Ye, M. Cinke, J. Han and M. Meyyappan, *Nano Lett.*, 2003, **3**, 929-933.